CORROSION SCIENCE AND TECHNOLOGY, Vol.23, No.6(2024), pp.495~502 pISSN 1598-6462 / eISSN 2288-6524
[Research Paper] DOI: https://doi.org/10.14773/cst.2024.23.6.495

# Current Challenges in AHSS from Galvanizing Process to In-Use Applications

**Ana P. Domingos[1,†] and Frank E. Goodwin[2]**

[1]*International Zinc Association, Brussels, B-1150, BE*
[2]*International Zinc Association, Durham, NC 27713, U.S.A*

(Received February 08, 2024; Revised June 06, 2024; Accepted June 11, 2024)

Automotive industry requirements for steels capable of enabling increasingly fuel-efficient vehicles continue to drive process technology of hot-dip lines worldwide. Advanced High Strength Steel and 3rd GEN zinc and zinc coated grades have reached stable and high process capability over the years. However, there is still much to be developed to increase their attractiveness to automobiles. Control of AHSS surface effects during annealing, use of computational tools to predict selective oxidation of alloy elements, decarburization of AHSS, and better use of Zn-alloys bath properties to improve AHSS galvanizability are motivations for continuous research development. Zinc-coated hot press-forming (PHS) grades have reached commercialization. Tailor-processed PHS could increase the efficient use of steel in automotive. A key barrier to adopting advanced zinc-coated steels is the reported incidence of liquid metal embrittlement and other performance challenges on non-fusion joining of Zn-coated steels. Regarding surface quality, there is much to learn in terms of the surface texture of incoming material with potential of offering galvanizing lines different alternatives that can minimize furnaces and Zn oxide defects after coating. Challenges in Zn-coated production, including improvement in productivity, quality, energy saving, and light-weighting, will be detailed discussed in this paper.

***Keywords:*** *AHSS, Third-generation steel, Welding, PHS, Zn Coatability*

## 1. Introduction

Advanced high-strength steels (AHSS) developed and commercialized in the past decade are designed to help automotive companies meet lightweight properties without compromising occupant safety requirements. These steel grades are expected to dominate the material share in automobiles, especially in body-in-white applications applicable to the EV market, in the foreseeable future. However, AHSS and 3G AHSS grades require special considerations and an understanding of their potential of galvanizability and forming behaviour to be even more successful in implementation in automotive manufacturing. Thus, it is imperative that 3G-AHSS compositions and processing routes have compatibility with CGL thermal processing capabilities and have as-annealed surfaces that can be reactively wetted by the Zn alloy bath such that adherent, high-quality coatings result.

It is well established that alloying elements such as Mn, Si and Cr will selectively oxidize in standard $N_2$-x$H_2$-y$H_2O$ CGL process atmospheres, which can result in poor reactive wetting and unacceptable coatings. Several techniques have been advocated for controlling the external oxide morphology, among the more successful of which are controlling the process atmosphere oxygen potential (pO2) such that internal oxidation occurs [1,2] and researchers continue work to understand better and mitigate external selective oxidation, the same happens for phenomena as decarburization on AHSS.

Hot press-formed automobile components such as rockers, lower B-pillars and hinge pillars are low to the ground and critical in contributing to providing crash protection. These locations are where components can benefit from the combination of galvanic and barrier protection offered by zinc-containing coatings. In recent years, steel strip galvanized with GI or GA have been studied as a second alternative for the coating of 22MnB5 steel in the hot press formed process, mainly for companies with conventional continuous galvanizing lines, in which the pots for the Al-Si coating are not available. The main advantage of Zn-based coating compared to AlSi coatings is the corrosion resistance, allowing applications to stamped parts that are exposed to high moisture content [3]. Two significant constraints

†Corresponding author: apdomingos@zinc.org

for hot press-formed steels that are zinc-coated are that no liquid zinc should be present during pressing, The presence of liquid metal originates during heating and soaking in the furnace, where the blank is subjected to a temperature of about 900 ºC while the pure zinc melt temperature is 419.5 ºC [4] is prone to the occurrence of LME (Liquid Metal Embrittlement). This phenomenon has required intensive effort of research to propose a successful mitigation alternative which avoids that a portion of the liquid zinc contacting the substrate, diffusing through the austenite grain boundaries acting as cracking, leading to brittle intergranular fracture [5].

Regarding the steel surface, AHSS and 3G-AHSS processed in continuous galvanizing lines are much more sensitive than lower-strength grades to variabilities in temperature during the thermal cycles used to prepare strip for dipping in the galvanizing bath. Much of this variability is caused by variations in the emissivity of the strip surface, which can promote errors in the furnace temperature measurement variations along the coil, leading to non-uniform mechanical properties on the final product. Computational simulations have been conducted to understand better the correlation between the emissivity versus annealing temperature over the length of AHSS grades, besides the influence of surface oxides on emissivity profile evolution.

This chapter provides a literature review combined with the most recent findings on GAP-Galvanizing Autobody Partnership on the investigation and contribution to the main challenges in galvanizing AHSS and 3G grades, such as selective oxidation, decarburization, and surface emissivity control. A discussion of new steel compositions for Hot Stamping possibly compatible with GI and GA coatings and further investigations on LME issues will also be presented.

## 2. Selective Oxidation, Decarburization and Effect on Galvanizability of AHSS

The three major problems associated with AHSS and 3G AHSS are selective oxidation and decarburization during inter-critical annealing and liquid metal embrittlement (LME) during either hot press forming (HPF) or resistance spot welding (RSW) [4] processes at the customer end. There have been many reports on understanding the mechanisms of coating overgrowth (in batch galvanizing), selective oxidation (in continuous galvanizing) and LME (in HPF and RSW) issues.

To prevent surface selective oxidation during galvanizing furnace pretreatment, before Zn dipping, advanced high-strength steels are increasingly subjected to an oxidation step prior to a reduction step that permits galvanizable surfaces to be presented to the galvanizing bath. Because the diffusion coefficient of oxygen from the surface into the bulk of many AHSS and 3G AHSS compositions is much higher than solute elements such as Mn, Si, Cr, and others that cannot be reduced if they reach the surface of the steel sheet, it is possible to immobilize a sufficient fraction of these elements in an internally-oxidized layer so that only a small portion reaches the steel surface [8], permitting the strip surface to be richer in Fe, which can be easily reduced from its oxidation states to a metallic state that can then be reacted with the galvanizing bath to produce acceptable-quality coatings. However, the high furnace atmosphere dewpoints used for internal oxidation can result in significant decarburization, over much longer distances in the steel because of the higher mobility of C. The emitted C combines with $O_2$ in the high dewpoint atmosphere. Together with the effects of decarburization on steel substrate properties, it can result in soot formation in the downstream furnace zone and carburizing of the refractory steels used in the radiant tubes in these zones [5]. The interaction between internal oxidation, both in grain boundaries and grain interiors and decarburization behavior in AHSS (dual-phase, TRIP and 3G) during CGL processing and its interaction with internal and external oxides were investigated on dual phase steels with 0.07%C, 2.5% Mn, 0,3%Si 0,15%Al,0.3%Cr, after piloted annealed at 800 ºC in $N_2$-5vol%$H_2$, with DP 0 ºC. The soaking time (from 0 to 120 s after reaching 800 ºC) and heating and cooling rate of 15 ºC/s. Fig. 1 demonstrates the correlation between internal oxidation and decarburization for the same experiments. The oxidation rate is very high, between 750 to 800 ºC, it then decreases to reach a plateau after 30 seconds annealing. After 50s of soaking, the oxidation depth reaches levels of 0.8 to 1.2 μm. The temperature eutectoid for γFe as starting point for this experiment as an arbitrary choice, considering the starting point for internal oxidation on Dual Phases material from 700 ºC [6].

An increase in the depth of the decarburization was observed front to the increase of the annealing time, the order of magnitude of decarburization depth as measured

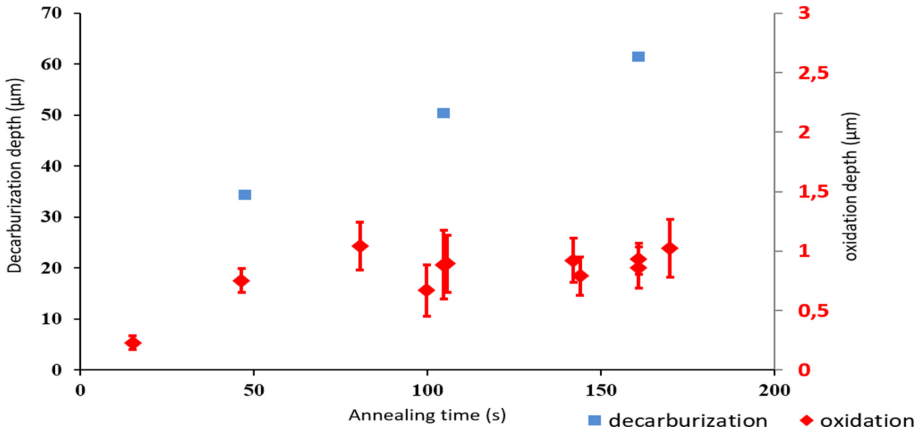


**Fig. 1. Correlation between internal oxidation and decarburization on Dual Phases samples annealed with 800 °C and 120 s annealing time**

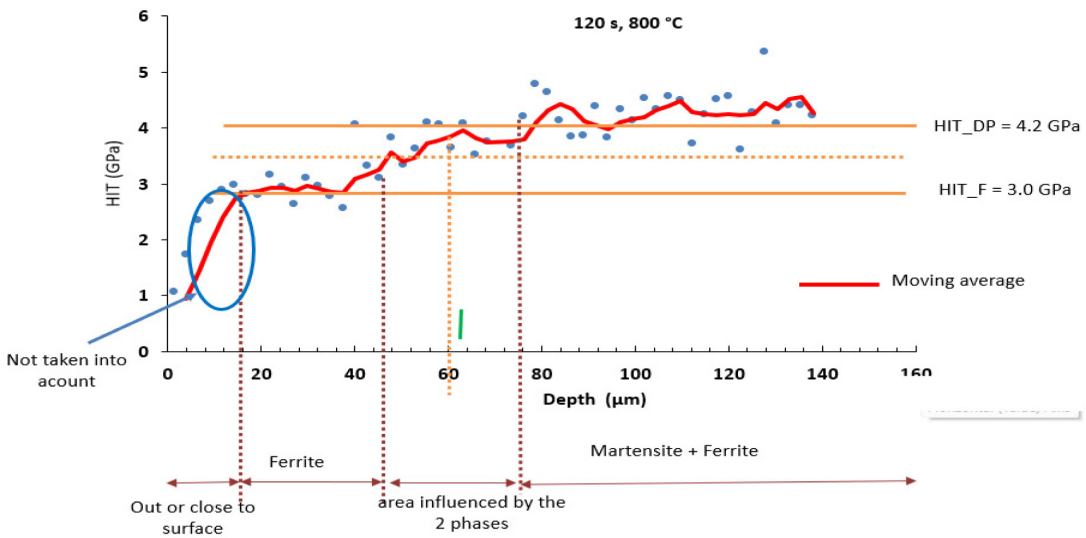


**Fig. 2. Hardness is presented here as a function of depth from the steel surface (depth 0) to the steel bulk**

at approximately 50 µm, while the order of magnitude of internal oxidation depth was 1 µm. The results predicted a small effect of surface oxides on decarburization for the experimented conditions. Also in GAP, was found that the decarburized thickness may be as high as 60 µm, but the samples used were much smoother than an industrial sheet. Higher dew points resulted in higher rates of decarburization. On the current experiments, the oxide formed on the surface did not present a significant barrier to decarburization. For the AHSS grade, C content down to a depth of 2 µm became sufficiently low to transform austenite into ferrite after soaking. During overageing, the developed model predicted that the C content in the ferrite and austenite close to the surface can increase by diffusion from the bulk; however, at the low overageing temperature of 450 °C the ferrite formed during decarburization may not transform back to austenite. Also, the martensite start temperature for many 3G sheets of steel is near this overageing temperature which can also influence the distribution of C. For the AHSS, the stronger decarburizing was coincident with less surface selective oxidation of Mn-Si, indicating that the internally oxidized layer formed during CGL processing was insufficient to block the flow of carbon out of the steel. By contrast, a greater degree of surface selective oxidation was coincident with less decarburization; however, this also coincided with a presumed higher-fraction coverage of oxides on the surface of the steel by the solute elements. In these oxidation/reduction treatments in AHSS with relatively high Si content, hematite was found to be the dominant surface oxide rather than the less compact wuestite

that was found on the DP steel. When soaking was made at 850 ºC with the AHSS grade, coating adhesion was always found to be acceptable, using the oxidation reduction process, even with 1% hydrogen in the reducing gas. Under this condition, carbon participated in iron oxide reduction at the surface at the expense of a more severe carburization of the near-the-surface volume.

Nanoindentation experiments were able to predict the hardness of the decarburization layer according to Fig. 2. Research is focused on the surface ferrite layer, the transition zone, and the martensite/ferrite bulk. The oxidation layer is too thin to be characterized by this technique. With nano-indentation, hardness is given by the force exerted by the indent divided by the surface area of the indentation left in the material. Hardness is measured on the cross-section of the steel sample as a function of distance from the steel surface, considering the hardness of the ferritic layer and the steel bulk. between the two, an increase in hardness due to the increase in the amount of martensite in the structure.

## 3. Hot Stamping Zn Coated AHSS

The use of press hardening steels (PHS) in automotive structural applications has increased significantly over the last decade. Current applications have focused mainly on safety-related applications such as roof rails, side impact beams and structural reinforcements, where the overall goal is to decrease the mass of the body-in-white while enhancing vehicle safety [7]. However, Zn-coated PHS can be susceptible to liquid metal embrittlement (LME) during direct hot stamping (DHS), and this has resulted in the wide-spread use of Al-Si PHS coatings, which form a series of solid Fe-Al-Si intermetallic during austenization [4] and, therefore, avoid LME during DHS. However, these Fe-Al-Si intermetallic coatings do not provide cathodic corrosion protection and are not compatible with the Zn-based primers commonly used in automotive assembly.

The main advantage of considering Zn-based coating also for hot stamping process is the corrosion resistance, allowing applications to stamped parts that are exposed to high moisture content balance, being α (Fe, Zn) in the coating is required to provide meaningful corrosion protection to the steel substrate [8]. Also, a minimum GI coating weight of 70 g/m$^2$ per side was required to obtain this level of the gamma ($Fe_3Zn_8$) in the final press-hardened coating. On GAP because of the need for gamma ($Fe_3Zn_8$) phase to provide cathodic protection in the coating, together with the requirement of heating the

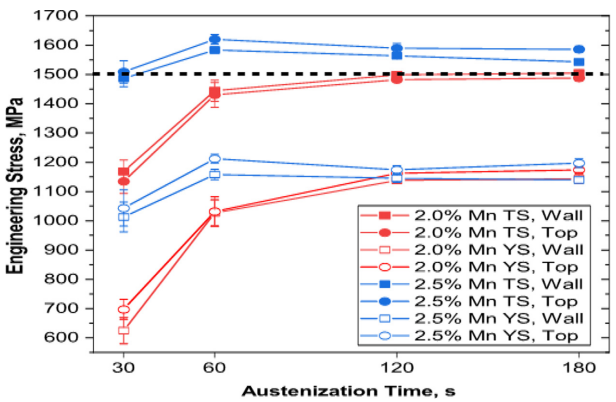


**Fig. 3. UTS curves for G samples, containing different percentages of Mn, hot pressed with an austenitization time of 180s [10]**

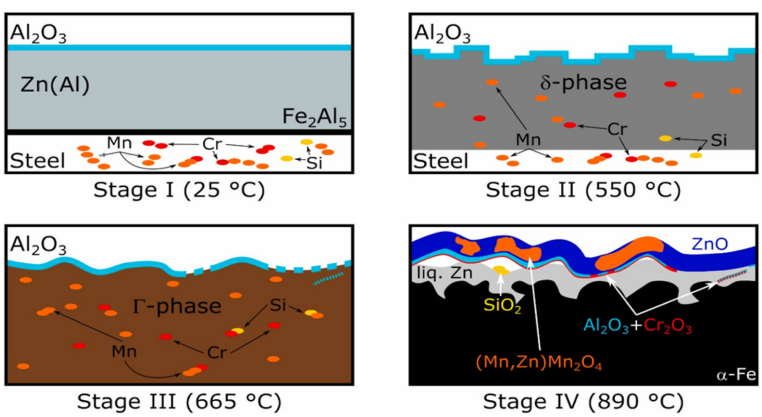


**Fig. 4. Schematic of four important oxide–forming stages during press hardening annealing showing only the dominant Fe–Zn phases and the main oxide–formation of Al, Zn and the main alloy elements [8]**

conventional 22MnB5 direct hot press forming grades to above 782 °C to give the required austenitization, it was investigated the development of two new grades, with 2.0 and 2.5% Mn, Fig. 3, shows the UTS results vs. austenitization time, proving that is possible to use either the 0.20C-2.0Mn-0.26Si-0.005B or 0.19C-2.5Mn 0.26Si-0.005B prototype grades to satisfy the objectives of UTS $\geq$ 1500 MPa and $\geq$ 15 vol% Γ-Fe3Zn10 for robust cathodic protection while avoiding LME. These grades can be austenitized in lower temperatures in hot stamping (550-650 °C), avoiding the occurrence of LME (>750 °C).

Also, in another GAP project was checked precursor GI and GA coatings were over a range of coating weights of interest and were processed using hot press forming heat treatment routes to produce a wide range of microstructures and final zinc compositions. It was concluded that a final coating that included a significant fraction of gamma ($Fe_3Zn_8$) phase (minimum 15 v%) with the main part of the oxide layer consists of ZnO, which eventually transforms to Zn $(OH)_2$ over time in ambient atmosphere. The dominant polycrystalline ZnO layer is accompanied by a spinel oxide (Mn, Zn) $Mn_2O_4$, where Mn and Zn substitute each other. Additionally, low amounts of Fe from the steel substrate were found along the spinel phases. A thin $Al_2O_3$ film, originating from low Al additions in the Zn bath, usually separates the primary oxide layer from Fe–Zn phases. Moreover, the oxide layer is often lifted off from the subjacent intermetallic Fe–Zn phases. Thus, the faint $Al_2O_3$ layer is attached to the bottom side of the oxide layer but not onto the intermetallic Fe–Zn phases. Additionally, phase transformations during austenitization annealing lead to volume changes, which can damage the otherwise closed $Al_2O_3$ coating. Remnants from these cracks are clusters of small $Al_2O_3$ particles and were found in the Γ–phase. If Cr is available from the steel alloy, it acts as an enhancement for Al, attaching to the Al2O3 layer and oxidizing to $Cr_2O_3$. Typically, Cr is not found on the surface, which suggests that it was already oxidized before annealing (e.g., by selective oxidation). During annealing, the $(Al,Cr)_2O_3$ layer behaves like a filter in the liquid Zn, which allows only Zn and Mn to pass through leading to the formation of oxides, but traps precipitates of other elements. Dilatometry work conducted on these two grades also showed that it was possible to obtain fully martensitic structures when they were cooled to temperatures less than 750 °C. Cooling rates for the 2.0% Mn steel must be at least 10 °C/s, and 5 °C/s for the 2.5% Mn steel, to produce fully martensitic microstructures. Another important investigation was done by Gaderbauer [8], he looked at the effects of steel alloying elements on the formation of the surface oxide layer of hot–dip galvanized press-hardened steel after austenitization annealing. For this, he examined samples of 22MnB5-GI 70/70, 20MnB8 GA 90/90, and 22MnCrB8-2 GA90/90. The main question was how the different alloy compositions influence the formation of the surface oxide layer during the annealing process. Focusing on the differences in the alloy and coating compositions, the investigated specimens can be divided into 2 × 2 groups. The first distinction was based on the coating type (GI or GA). A second distinction was made with respect to the alloy composition. 20MnB8 are steel grades with no Cr as an alloying element, while 22MnB5 and 22MnCrB8–2 contain low amounts of Cr. The results show that for the range of either GI and GA and for the tested chemical compositions, the oxide formation in the hot press furnace occurs according to the scheme of Fig. 4.

## 4. Emissivity Control on AHSS during Annealing

Regarding annealing AHHS and 3G-AHSS grades, improvements in pyrometry for the measurement of strip temperature at soaking temperature are still required. [10]. Industrial multi-wavelength pyrometers typically provide a temperature estimate by combining the thermal radiation emitted from the steel with an emissivity compensation algorithm that predicts the emissivity of the steel [11]. The emissivity of AHSS is known to vary with wavelength, surface roughness, and alloy composition and evolves during annealing in a manner that depends on temperature profile, dewpoint, and other process parameters [12]. Additionally, newer AHSS alloys include elements that form stable oxides on the steel surface, further inducing variations in the emissivity of the steel [13]. The interdependent effect of these factors combined with non-uniform radiative properties across the length and width of the incoming cold-rolled coil [14] makes it difficult for existing compensation algorithms to provide the precise emissivity estimates required for accurate pyrometry of AHSS. Compared to other metals and alloys [15,16], there

is little information available on the in-situ emissivity of AHSS and how it changes with temperature and other process parameters such as dewpoint, especially at the near-infrared wavelengths critical for pyrometry. Recent experimental and theoretical studies on dual-phase DP780 and DP980 alloys [16] have established that the spectral emissivity of these alloys varies with the combined effects of wavelength, dewpoint, alloy-composition (in terms of silicon-to-manganese ratio), and surface roughness. The spectral emissivity at the shorter pyrometry wavelengths (≤2.5 μm) is strongly influenced by the structure of the oxide layer formed on the surface, which in turn depends on the quantity of the alloying elements and their interaction effect with the annealing atmosphere. Recent work on GAP focused on the explanation of how the radiative properties evolve with temperature during intercritical annealing and developing a model that effectively captures interdependent variations in spectral emissivity [17].

**Table 1. Dewpoint and Oxygen Concentration for the Annealing Atmospheres**

| Target dew point (°C) | Actual dew point (°C) | Oxygen concentration (ppm) |
|---|---|---|
| -30 | -30.68 | < 5 × 10−21 |
| -10 | -9.59 | < 5 × 10−21 |
| +10 | +10.16 | 3.17 × 10−21 |

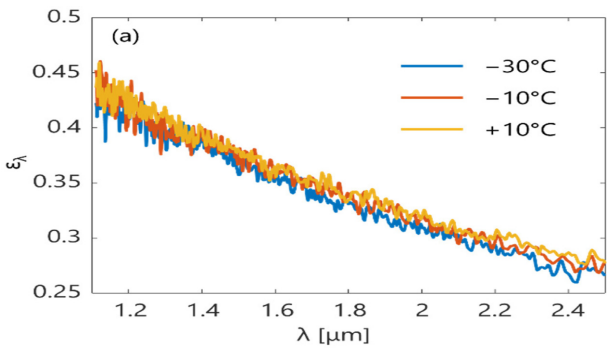


**Fig. 5. Pre-annealed spectral emissivity, ελ, for the DP980 coupons**

### 4.1 Emissivity variations under different dew point conditions:

The experiments aiming to observe how emissivity varies under different dep point conditions during annealing were conducted with a cold-rolled DP980 (1.5 mm) alloy having a (Si/Mn) ratio of 0.04 and roughness of the as received mid-coil steel surface is *R*q = 0.65 μm, as measured with an optical profilometer. The samples were annealed in a vacuum-grade thermal processing chamber designed for optimum control over the oxygen content of the annealing atmosphere. Table 1 lists the actual dewpoint and oxygen concentration values measured at the start of the experiment.

The as-received spectral emissivity of each coupon was characterized at room temperature by the spectrometer. The nearly identical emittance spectra of the as-received steel in Fig. 5 indicate that the coupons all share a similar pre-annealed surface state.

Fig. 6 shows how the in-situ time-resolved spectral emissivity evolves with the annealing temperature and time in comparison to the pre-annealed surface state. The pre-annealed spectral emissivity in Figs. 6a – f represents the average of the three spectra shown in Fig. 5. The observed variations in spectral emissivity are linked to the interdependent effect of dewpoint and temperature on the oxidation of metals. The measurements in Fig. 6a show that the resulting oxide topography, irrespective of dewpoint, influences the rate at which the spectral emissivity changes with wavelength, as evident from the drastic change in the slope compared to the pre-annealed state.

Based on the oxygen potential diagram for this DP980 alloy, all three dewpoints analyzed in the present study favor the segregation and selective oxidation of Si, Mn, Cr, and Si from the bulk metal. However, the degree of internal/external selective oxidation, as well as the properties of the resulting oxide layer, depends on the thermodynamics and kinetics of the oxidation reaction [13,18]. Therefore, as the samples heat up from their pre-annealed state to 400 °C, the sample processed at higher oxygen partial pressure (i.e., +10 °C dewpoint) would have a significant amount of both internal and external oxides, which would result in a significant increase in spectral emissivity observed. Consequently, the change in emissivity is reduced with the reducing oxygen partial pressure at the lower dewpoints (−10 °C and −30 °C) due to the formation of the thinner external oxide films. Beyond 400 °C in Figs. 6b ~ g, the spectral emissivity decreases with increasing temperature at all three dewpoints.

Given that spectral emissivity is a surface property and that the surface of annealing AHSS is best described as

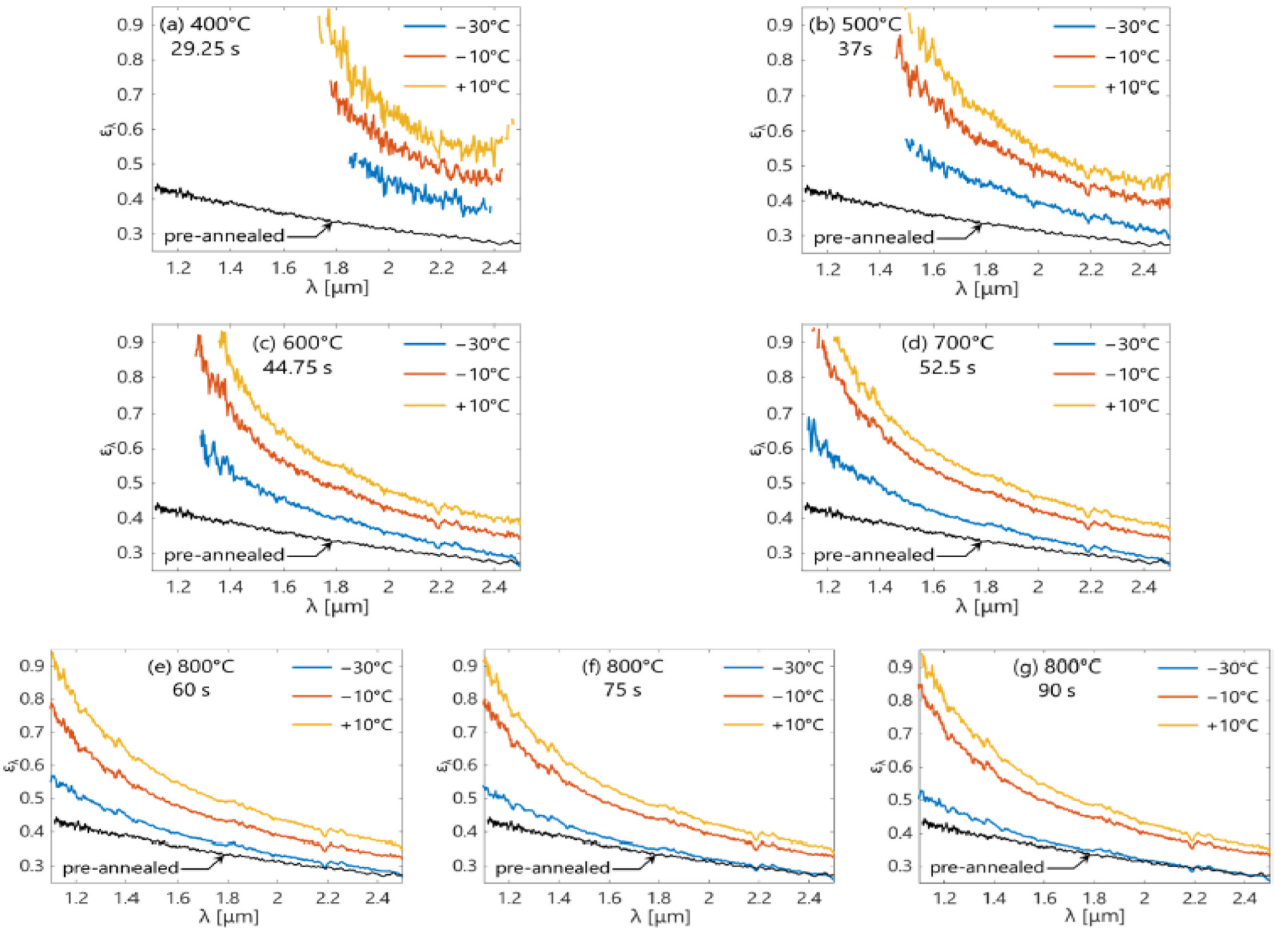


**Fig. 6. Measured spectral emissivity for the three experimented dewpoints as a function of the annealing temperature and time. (a) 400 °C - 29.25 s, (b) 500 °C - 37 s, (e) 600 °C - 44.75 s, (d) 700 °C - 90 s, (e) 800 °C - 90 s (soak starts), (f) 800 °C - 75 s (mid soak), and (g) 800 °C - 90 s (soak ends)**

a metallic oxide, it follows that the spectral emissivity of these DP980 coupons will decrease with increasing temperature. The sample annealed at the lowest dewpoint (−30 °C) undergoes the largest drop in spectral emissivity with increasing temperature. At the 800 °C peak annealing temperature (PAT) shown in Figs. 6e – g, the spectral emissivity of the −30 °C sample approaches its pre-annealed value for wavelengths longer than 2 μm. This suggests that the external oxide layer may undergo reduction at these higher surface temperatures.

## 5. Conclusions

Based on this overview of different challenges for processing AHSS and 3G steels in continuous galvanizing lines, the following conclusions can be reached:

1. No correlation was observed on Dual Phase with 0.07%C, 2.5% Mn, 0,3%Si 0,15%Al,0.3%Cr, after piloted annealed at 800 °C in $N_2$-5vol.%$H_2$, with DP 0 °C, between internal oxidation and decarburization. The Decarburization increased over annealing time, achieving a max. of 60 μm after 150 s. The internal selective oxidation performed as plateau profile over annealing time, with an average of 1 μm.

2. Based on discussed experiments on pre-hardening, the prototype Zn-coated 0.20C - 2.5Mn press hardening steel, it was determined that the minimum target UTS of 1500 MPa was realized whilst providing a Zn-based coating with robust sacrificial cathodic protection potential. A prediction under oxide formation during hot stamping experiments on Zn-coated 0.20C-2.5Mn press hardening steel was also predicted.

3. The paper also proposed an in situ-based stochastic emissivity model that provided robust estimates for the peak

annealing temperature irrespective of the dewpoint. The results obtained with the stochastic approach highlight the benefit of estimating a measure of uncertainty alongside the nominal temperature estimate. With knowledge of the inherent uncertainty introduced by the imperfectly known emissivity, steelmakers can compare the posterior estimates against predefined temperature tolerances for AHSS during intercritical annealing.

## References


1. D. Ximenes, L. P. Moreira, J. E. R. Carvalho, D. N. F. Leite, R. G. Toledo, F. M. S. Dias, Phase transformation temperatures and Fe enrichment of a 22MnB5 Zn-Fe coated steel under hot stamping conditions, *Journal of Material Research and Technology*, **9**, 629 (2020). Doi: https://doi.org/10.1016/j.jmrt.2019.11.003
2. T. Prosek, *Proc. EGGA Assembly 2017 Conf.*, Towards Corrosion Resistant Zinc-Based Coatings Through Alloying and Microstructural Optimization, Prague (2017).
3. A. R. Marder, The metallurgy of zinc-coated steel, *Progress in Materials Science*, **45**, 191 (2000). Doi: https://doi.org/10.1016/S0079-6425(98)00006-1
4. S. M. A. Shibli, B. N. Meena and R. Renya, A review on recent approaches in the field of hot dip zinc galvanizing process, *Surface and Coatings Technology*, **262**, 210 (2015). Doi: https://doi.org/10.1016/j.surfcoat.2014.12.054
5. L. Gong, N. Ruscassier, P. Chrétien, P. Haghi-Ashtiani, L. Yedra, M.-L. Giorgi, Nucleation and growth of oxide particles on a binary Fe-Mn (1wt.%) alloy during annealing, *Corrosion Science*, **177**, 108952 (2020). Doi : https://doi.org/10.1016/j.corsci.2020.108952
6. N. Gao, W. Sun, J. Smiley, and Y. Liu, *Proc. 9th International Conference on Zinc and Zinc Alloy Coated Steel Sheet (Galvatech 2013)*, pp. 61-67, The Chinese Society for Metals, China (2013).
7. J. R. McDermid, C. Dever, S. Kheiri, C. Thomsen and F. E. Goodwin, Development of a High-Mn-Containing PHS for Liquid Metal Embrittlement Resistance, Proc. International Symposium on New Developments in Advanced High-Strength Sheet Steels Vail, Procuct Code. PR-298-031, Colorado, USA (2023). Doi: https://doi.org/10.33313/298/031
8. J. M. Buyn, S.-R. Bang, H. W. Kim, T.-Y. Kim, S.-J. Hong, Y. D. Kim, Effect of heat treatment on corrosion resistance and adhesion property in Zn-Mg-Zn multi-layer coated steel prepared by PVD process, *Surface and Coatings Technology,* **309**, 1010 (2017). Doi: https://doi.org/10.1016/j.surfcoat.2016.10.043
9. J. McDermid, Galvanized Autobody Partnership Project ZCO-70- Presentation to GAP Review Meeting in Paris, International Zinc Assn. Durham, USA (2022).
10. A. R. Marder and F. Goodwin, The Metallurgy of Zinc Coated Steels, p. 24, Elsevier, United States (2023).
11. A. Araújo, Multi-spectral pyrometry—a review, *Measurement Science and Technology*, **28**, 082002 (2017). Doi: https://doi.org/10.1088/1361-6501/aa7b4b
12. F. Tanaka and D. P. Dewitt, *Proc. National Heat Transfer Conf.*, pp. 69 − 75, ASME: Philadelphia, Pennsylvania (1989).
13. R. Khondker, A. Mertens, and J. R. McDermid, Effect of annealing atmosphere on the galvanizing behavior of a dual-phase steel, *Materials Science and Engineering: A*, **463**, pp. 157 − 165 (2007). Doi: https://doi.org/10.1016/j.msea.2006.09.116
14. N. S. Narayanan, K. Lin, F. K. Suleiman, and K. J. Daun, The causes and effects of preannealed radiative property variations across full-hard advanced high-strength steel coils, Steel research international, **94**, 2200705 (2023).
15. P. Hagqvist, F. Sikström, and A.-K. Christiansson, Emissivity estimation for high temperature radiation pyrometry on Ti–6Al–4V, *Measurement*, **46**, 871 (2013). Doi: https://doi.org/10.1016/j.measurement.2012.10.019
16. Q. Somveille, P. Mosser, M. Brochu and K Daun, *Proc.11th International Conference on Zinc and Zinc Alloy Coated Steel Sheet, (Galvatech 2017)*, pp. 210 – 217, ISIJ, Tokyo, Japan (2017).
17. F. K. Suleiman, N. S. Narayanan, K. J. Daun, *Proc. Iron & Steel Technology Conf. (AISTech 2023)*, pp.1598 - 1607, Detroit, Mich., USA (2023).
18. L. Cho, G. S. Jung, and B. C. De Cooman, On the Transition of Internal to External Selective Oxidation on CMnSi TRIP Steel, *Metallurgical and Materials Transactions A*, **45**, 5158 (2014). Doi: https://doi.org/10.1007/s11661-014-2442-7